RSC Advances

ROYAL SOCIETY OF CHEMISTRY

www.rsc.org/advances

Journal Name

ARTICLE

Epitaxial growth of highly infrared-transparent and conductive $CuScO_2$ thin film by polymer-assisted-deposition method

Received 00th January 20xx,
Accepted 00th January 20xx

DOI: 10.1039/x0xx00000x

www.rsc.org/

Ya-Hui Chuai, Hong-Zhi Shen, Ya-Dan Li, Bing Hu, Yu Zhang, Chuan-Tao Zheng*and Yi-Ding Wang*

As an important wide bandgap p-type conductive delafossite material, $CuScO_2$ (CSO) has been intensively investigated for its wide applications in multi-functional optoelectronic devices. In order to obtain both high infrared (IR) transparency and low resistivity, we report on, for the first time, the experimental preparation of single phase epitaxial CSO thin film by using polymer-assisted-deposition (PAD) method. As a key point in the PAD process, the used polymer materials (PEI and EDTA) not only control the desired viscosity for the process, but also bind the metal ions to prevent premature precipitation and formation of metal oxide oligomers. The technique results in a homogeneous distribution of the metal precursors in the solution as well as the formation of uniform metal organic film. Due to the uniaxial locked epitaxy mechanism, the epitaxial growth of CSO (0001) thin film on a-plane sapphire is achieved, and the orientation relationship of the film with respect to the substrate are confirmed to be CSO[3R](0001)//a–$Al_2O_3(11\bar{2}0)$. The obtained CSO thin film from the PAD technique exhibits a low electrical resistivity of 1.047 Ω•cm at room temperature, and a high transmittance of 65-85% in the near-IR range and more than 85% in the mid-IR range. The presented technique does provide the possibility of preparing high-crystallinity oxide films which can be applicable over a wide wavelength rangefromvisible band to infrared band.

1 Introduction

Transparent conductive oxides (TCOs) have been widely used in optoelectronic devices, such as flat panel displays, solar cells and organic light-emitting diodes, etc.,[1-3] because of their high electrical conductivity, excellent optical transmittance in the visible light region and unlimited scalability. The previous well-known materials are all-electron-doped n-type oxides, such as Al-doped ZnO, Sn-doped In_2O_3 and Sb-doped SnO_2. However, due to limited natural abundance, relatively high reflectivity and limited infrared (IR) transparency of for these oxides, their applications are severely restricted in the next generation of optoelectronic devices. Transparent conductors with high infrared transmittance have drawn much attention for applications in infrared imaging and sensing, infrared emission devices, modulators and switches for fibre-optic communications, and IR-sensitive solar cells.[4] In order to fully apply the transparent conductive oxides into the transparent optoelectronic devices, developing electrical conducting films that are transparent in the infrared region, has been of growing interest.

As an important class of wide bandgap transparent p-type conductive delafossite materials, $CuMO_2$ (M = Al, Cr, Fe, Ga, In or Sc) has been intensively investigated in the last few years for their transparency in the visible range.[5-9] The $CuMO_2$ structure is an inherently low dimensional structure, which is composed of Cu_2O dumbbell layer, edge-sharing MO_6 octahedron layer, existence of 3d orbitals, and vacancy of Cu ion and interstitial oxygen atoms. Consequently, the Cu^+-based delafossite oxides exhibit p-type conductivity and unique optical properties due to such structure. Among these delafossite compounds, we are more interested in $CuScO_2$ (CSO), which is one of the p-type Cu^+-based delafossite oxides with the smallest Cu–Cu distance and the possibility of excess oxygen intercalation.[10] The Cu–Cu distances significantly influence the electrical conductivity in Cu^+-based delafossite oxides, because holes predominantly pass through the Cu^+ planes.[11] Therefore, the CSO would exhibit higher p-type conductivity than other Cu^+-based delafossites. Moreover, the CSO film has a direct-transition wide bandgap (~3.7 eV), which is obviously different from other delafossite oxide films.[12] Thus, the CSO film has already been a crucial potential material for infrared optoelectronic applications.

Up to now, a few attempts have been tried for the synthesis of CSO thin film. The first one is physical vapour deposition (PVD), which is a widely-used technique, though some properties, such as high capital cost and relatively small coating area, are still unsatisfied.[13] Yoshiharu Kakehi et al. have reported single phase CSO thin film deposited by pulsed laser deposition (PLD), and the resulting film showed an optical transmittance of larger than 65% in the visible region, and an estimated resistivity of 9.3×10^6Ω•cm at room temperature.[14] Yuya Matsubara et al. developed tri-phase epitaxy (TPE) method to grow high crystallinity CSO thin film by employing molten Bi–O flux on the growth surface.[15] Chemical deposition is another well-known method for the growth of thin films with effective-cost and large-area. However, the reported

State Key Laboratory on Integrated Optoelectronics, College of Electronic Science and Engineering, Jilin University, 2699 Qianjin Street, Changchun 130012, PR China
* Corresponding authors. Email: zhengchuantao@jlu.edu.cn (C.-T. Zheng); ydwang@jlu.edu.cn (Y.-D. Wang)

solution-based methods of preparing $CuMO_2$ films always face many technical challenges, such as the formation of unwanted phases.[16] Besides the above two techniques, an alternative synthesis route, named polymer-assisted deposition (PAD) technique, is technologically relevant to advance transparent electronics, and it has proven to be a powerful technique to grow both simple and complex metal-oxide thin films.[17] In this paper, we grow the single phase epitaxial CSO thin film on a-plane sapphire substrate and investigate its IR-transparency and conductivity in detail. As a key point in this process, the used two soluble polymer materials (PEI and EDTA) play a significant role in preparing high quality metal oxide films. Firstly, the formation of covalent complexes between the lone pairs on the nitrogen atoms of the polymer and the metal cations makes it possible to achieve a pure precursor solution by the commonly available chemical solution deposition techniques. This feature makes it feasible for physical filtration to remove unbound low molecular weight cations or anions. Secondly, the polymers control the desired viscosity for the process. Lastly, the polymers bind the metal ions to prevent premature precipitation and formation of metal oxide oligomers.The results are a homogeneous distribution of the metal precursors in the solution and the formation of uniform metal organic films. To the best of our knowledge, this is the first report for the epitaxial growth of singlephase CSO film by using the PAD method.

2 Experimental methods

2.1 Preparation of precursor solution

The precursor solution for the growth of CSO thin film was prepared by mixing two separate aqueous solutions of Cu and Scbound to polymers.Separate solutions were prepared using high purity(> 99.9%) metal salts copper (II) nitrate and scandium (III) nitrate. The polymers used in the experiment are polyethyleneimine (PEI) and ethylenediaminetetraaceticacid (EDTA), which were purchased from Alfa Aesar Corporation of china. Water used in the solution preparation was purified using the Milli-Q water treatment system. Ultrafiltration was carried out using Amicon stirred cells and 3000molecular weight cut-off, flat cellulose filter disks (YM3) under 65 psi (1 psi = 6.89 kPa) nitrogen pressure. In detail, copper nitrate (99.9%, 2.4 g) was first dissolved in 40 mL deionized water, followed by adding 3 g PEI polymer into the solution. Scandium nitrate (99.9%, 2.3 g) was dissolved in 40 mL deionized water, followed by adding 4 g EDTAinto the solution, after which 3g PEI was then added into the solution.The Cu and Sc solutions were then separately filtrated and concentrated in an Amicon filtration unit to give a final concentration of 250 mM for Cu and 250 mM for Sc, respectively. The polymers used in the PAD process should be soluble and compatible with the metal precursors, and also should undergo a clean decomposition upon heating. PEI is a kind of soluble polymer, which can decompose into small gaseous organics above 250 °C and leaves little or no residual carbon in the film with further increasing temperature. Moreover, it is well known that the first row transition metal Cu bind well to the simple PEI polymer, schematically in a manner as shown in Fig. 1(a). As for the hard-to-bind metal ions, such as Sc, the EDTA can play a big role. The major advantage of the EDTA is that it can form stable complexes with almost all metals, and then the EDTA complexes bind to the PEI via a combination of hydrogen bonding and electrostatic attraction, as show in Fig. 1(b). So PEI and EDTA are preferred polymers in our research. All the stabilization of these two metal ions in the solution, easily mixed according to molar ratio, allows the cations to react with one another to form the desired compound.

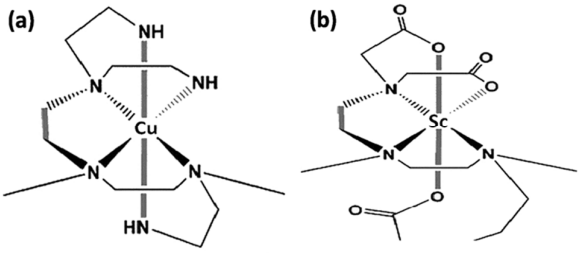

Fig. 1. Schematic illustration of chemical coordination of (a) Cu ion and PEI, (b) EDTA and PEI by hydrogen bondingand electrostatic binding.

2.2 Preparation of CSO thin film

The precursor with the desired stoichiometric ratio formed by mixing the above solutions was spin coated onto a-plane sapphire substrate at 3000 rpm for 30 s, then the Cu-PEI and Sc-EDTA-PEI mixing solution was spin coated on the substrate to form a homogeneous film. The obtained film was baked at 300 °C in air for 30 min, in order to remove the polymers. This process probably results in copper oxide and scandium oxide. The resulting film was annealed at 1050 °C for 1 h in flowing N_2, and then natural cooling to room temperature. This annealing process is actually a reaction procedure between copper oxide and scandium oxide, which generates CSO due to the mole ratio between Cu and Sc. Note that, during fabrication, the spin coating and baking process were repeated for six times to get a reasonable film thickness.

The thickness of the CSO film can be controlled through the following three factors: (a) the concentration of metal ions in solution, (b) spin speed, and (c) the number of spin-coating layer. Besides, the solution viscosity also has great influence on the film formation. Generally speaking, the larger the viscosity is, the slower the deposition rate becomes. On the contrary, if the viscosity is too low, the bad adhesion between solution and substrate is not beneficial to the formation of the film.

2.3 Characterization and measurement

The crystallographic orientation of the CSO thin film was characterized using conventional X-ray diffraction(XRD) technique with a Bruker D8 Advance X, Pert diffractometer (Cu-Kα : λ = 1.540 Å).The scanning speed was 4°/min from 10°to 70°.The surface chemical states were investigated using X-ray photoelectron spectroscopy (XPS, ESCALAB 250). The surface morphology of the film was examined byJSM-7500F field emission scanning electron microscope (FE-SEM), and an atomic force microscope (AFM) instrument (Veeco DI-3100) was used to further observe the microstructure. The surface and atomic structure of the film was also investigated using a high-resolution transmission electron microscope (HRTEM, TEM 2010F). The optical properties such as

the transmission and the absorptionof film were measured using an UV–VIS–NIR spectrophotometer (Shimazu UV-3600PC) in the wavelength range of 250–3000 nm and Fourier transform infrared spectrometer (FTIR) in the range of 400 to 4000 cm^{-1}. The electrical properties of the thin filmwere determined using aHall-effect measurement system (ACCENT HL55OOPC) between 90 and 300 K.

2.4 Sample preparation for HRTEM measurement

The polymethyl methacrylate (PMMA)-assisted method was used to divert the CSO film sample from the substrate for HRTEM measurement. First, a PMMA layer was spin coated on the surface of the sample, and then the sample was baked on the heating plate for 5 minutes. A piece of scotch tape larger than the sample was used as the support: open a window in the middle of the tape smaller than the sample surface; stick the tape on the surface of the sample; make sure that the sample surface can be seen through the window; make the tape be of the same size with the sample by cutting the edge part of the tape. Soak the sample in 5% HF solution for 1-hour-etching. After that, the PMMA layer supported by the tape was gently stripped from the substrate with a needle. The PMMA layer was rinse in deionised water, and then posted on a Cu mesh used in the HRTEM measurement. The Cu mesh was baked under an infrared lamp for 5 minutes to make the PMMA film and the Cu mesh bind together. Remove part of the PMMA film which is larger than the Cu mesh. Finally, the PMMA was removed with hot acetone, and the TEM test can normally be carried out.

3 Results and discussion

3.1 Structure and chemical valence characteristics

Fig. 2 (a) shows the XRD patterns of the prepared CSO film. As can be seen, well defined and high intensity (0003), (0006), (0009) and (0012) reflections are the only peaks in the scanned range from the CSO film, in addition to the substrate peak. The appearance of only (000l) diffraction peaks indicates that the film is preferentially oriented along the *c*-axis perpendicular to the substrate surface. It should be noted that no other detectable phases were observed. The full width at half-maximum (FWHM) of the (0009) rocking curve (Fig. 2(b)) is about 0.171°, suggesting good crystallinity of the film. From the d–spacing's of the (0006) peak, the lattice parameters a = 3.210(3) Å and c = 17.087(2) Å were determined for the CSO film, which are in quite good agreement with a = 3.216 Å, c = 17.089 Å (JCPDF#79-0599 CSO[3R]).

Fig. 3 shows the Cu-2p, Sc-2p and O-1s X-ray photoelectron spectra (XPS) of CSO thin film. In the Cu-2p spectrum, two distinct and intense peaks with binding energy of Cu-$2p_{3/2}$= 932.5 eV and Cu-$2p_{1/2}$ = 952.3 eV are observed, consistent with the Cu_2O (Cu^+) phase. Hence, the Cu ions are concluded to be in the monovalent state.[18] Fig. 3(b) shows two strong peaks in the Sc-2p spectrum at 401 eV and 406 eV for $2p_{3/2}$ and $2p_{1/2}$ peaks, respectively, which indicates that the valence state of Sc ions is +3, by compared with the National Institute of Standards and Technology (NIST) X-ray Photoelectron Spectroscopy Database. The O-1s spectrum of CSO films is centred on 530.2 eV in this study, implying −2 valence state. According to the XPS analysis, the Cu, Sc and O chemical states of CSO film are +1, +3 and −2 valence states, which support the formation of a pure CSO phase.

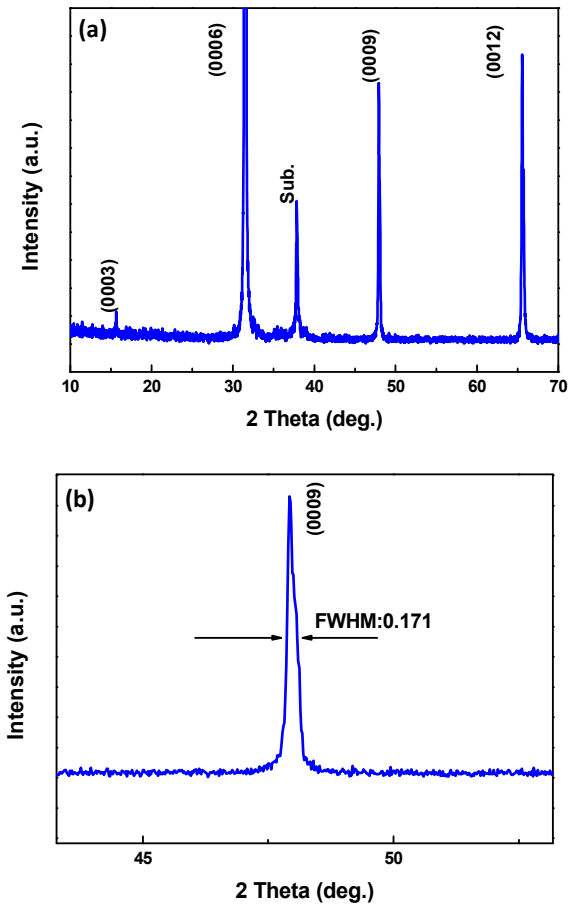

Fig. 2. (a) XRD patterns of the CSO film. (b) Enlarged XRD pattern of the CSO film at (0009) peak.

3.2 Morphologies and microstructure of the CSO film

Figs. 4 (a) and (b) show the surface and cross-sectional morphology of the CSO film. As can be seen from the Field emission scanning electron microscope (FESEM) images, the film is dense and uniform with no detectable micro-cracks. Additionally, the CSO film is tightly attached to the substrate and the thickness of film is uniformity which is approximately 240 nm. Fig. 4(c) shows the Atomic force microscope (AFM) image of the CSO film, the microstructure of grains with an average size of 100 nm are observed. The nano-particles arrange orderly, and the roughness of surface is about 20 nm, which is approximately 8.3% of the film thickness. This surface morphology implies that each grain corresponds to a single-crystal grain that has grown epitaxially on the substrate. High resolution transmission electron microscopy (HRTEM) image and selected area diffraction (SAD) pattern of the film are shown in Fig. 4(d). Stripe lines of ions at intervals of 4.2 Å and 7.8 Å are clearly visible, which corresponds to the d-spacings $(1\bar{2}10)$ and $(10\bar{1}0)$ in the CSO. The SAD pattern shows that the CSO thin film is a single crystal with the c-axis orientation perpendicular to the surface of the

a-plane sapphire substrate, each diffraction spot was assigned as $(10\bar{1}0)$ and $(1\bar{2}10)$.

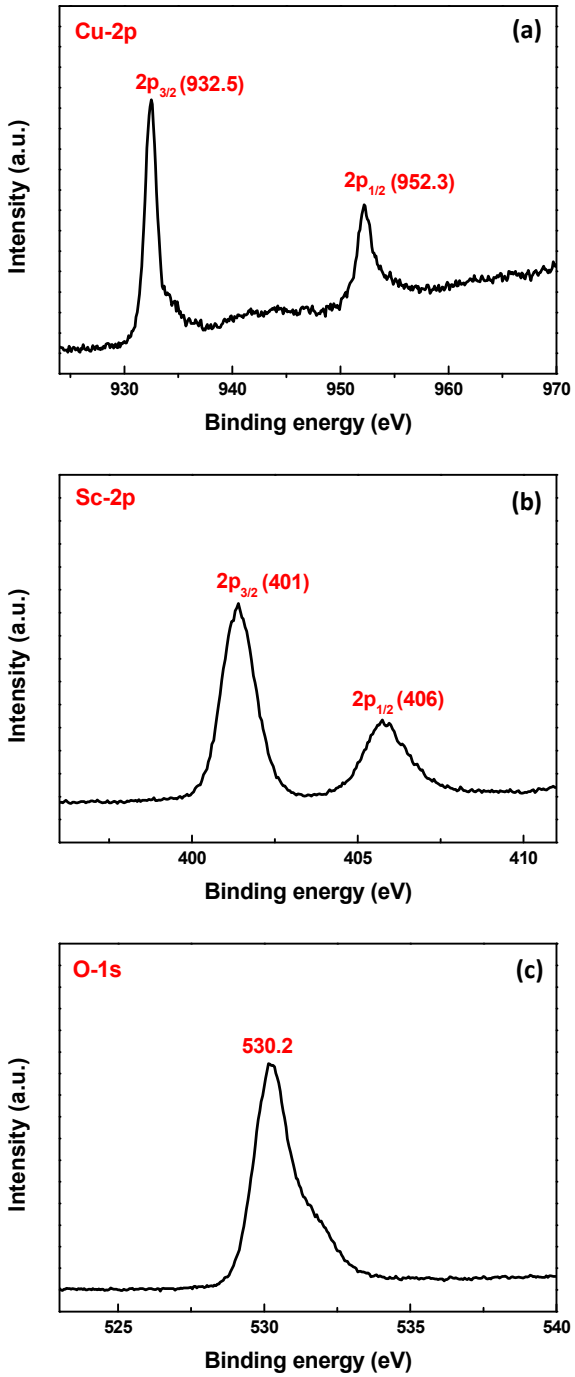

Fig. 3. X-ray photoelectron spectra of CSO thin film, (a) Cu-2p, (b) Sc-2p and (c) O-1s.

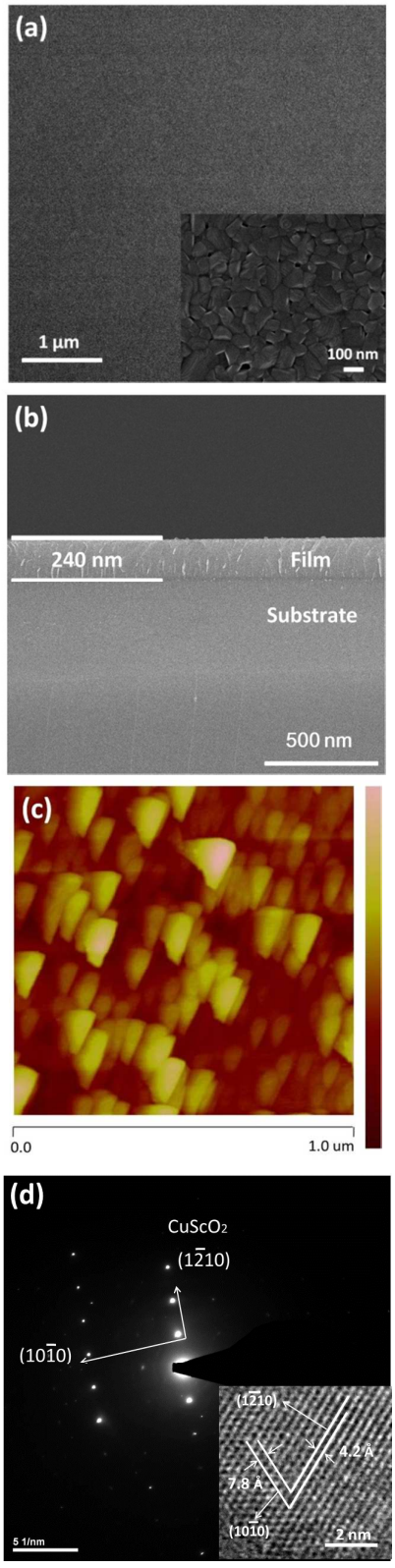

Fig. 4. SEM images of (a) surface morphology and (b) cross-sectional of the epitaxial CSO film; (c) AFM image of CSO film; (d) HRTEM image and SAD pattern of CSO thin film.

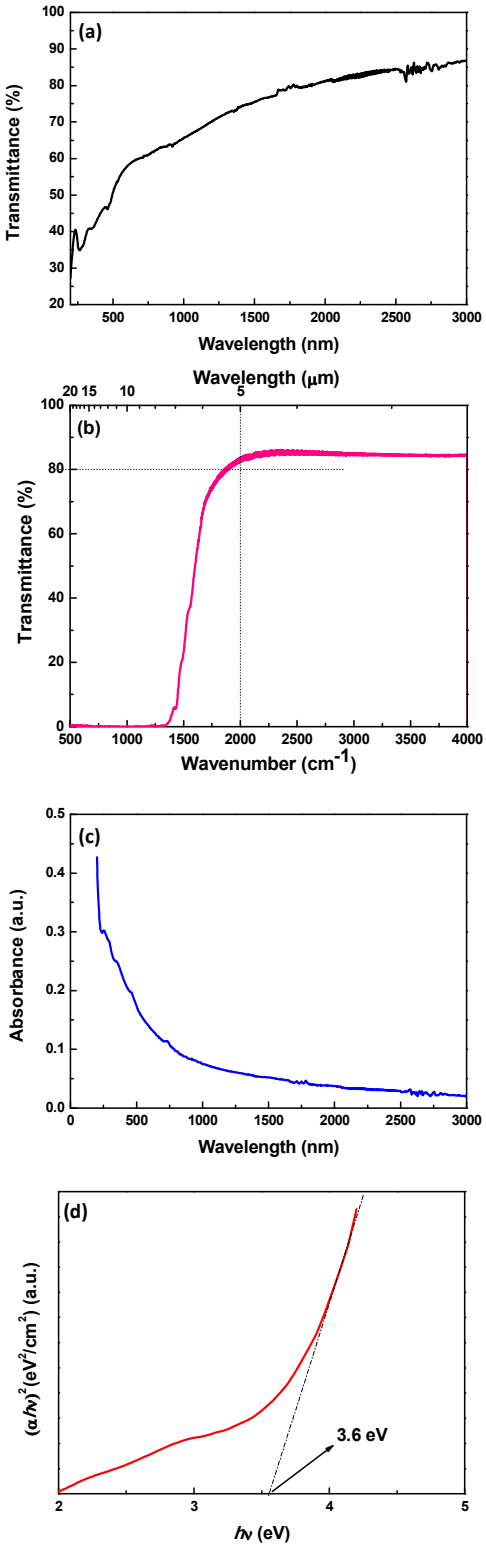

Fig. 5. (a) Optical transmission spectrum of CSO film, (b) Infrared transmission spectra of CSO film, (c) absorption spectrum of CSO film, and (d) $(ahv)^2$ versus hv plot.

3.3 Optical measurements of the film

Fig. 5(a) shows the optical transmission characteristics of the CSO film. The data were presented by subtracting the contribution of substrate. The film has an optical transmission of 40–65% in the whole visible range, and also shows high transmission of 65–85% in the near infrared spectral region. The reason that this film has a low transmittance over the visible region is probably due to the bandgap between the valence band maximum (VBM) and the first conduction band is ~3.0 eV for CSO, this narrow bandgap will result in an absorption in the visible range, which leads to a low transmittance in this band. The experimental optical band gap of CSO is likely to be between VBM and the second conduction band.[19] Fig. 5(b) shows that the CSO film has a total transmittance of more than 85% in the wavelength range 2.5–6 μm, without any sharp absorption features. The high transmittance (or low absorption), particularly in the mid-infrared region, is mainly due to the free-carrier plasma edge located in the far-infrared frequency.[20] The sudden decrease in the transmittance starting at 6 μm is due to collective oscillations of the conduction band electron, which is known as plasma oscillations. For the CSO film, when the frequency of the incident electromagnetic wave is equal to the free-carrier plasma oscillation frequency ω_p, the whole free-carrier will resonate, which leads to the increase of free-carrier absorption and the mutation of the material properties. If the frequency of the incident electromagnetic wave is lower than ω_p, most of the light will be reflected by the film resulting in a low transmittance; if the frequency is higher than ω_p, most of the light will propagate through the film resulting in a high transmittance. Therefore, ω_p determines the low cut-off frequency of transmission band.

Fig. 5(c) shows the absorption spectrum of CSO film. A sharp absorption edge is observed around the wavelength of 300 nm. The fundamental absorption, which corresponds to the electron excitation from the valence band to the conduction band, has been widely used to determine the optical bandgap of semiconductor materials. The relationship between the optical absorption coefficient (a) and the photon energy (hv) can be expressed as

$$ahv = A(hv - E_g)^m \quad (1)$$

where A is a constant, E_g is the optical bandgap of the materials, and m depends on the type of transition: m = 1/2 for direct band transition, m = 2 for indirect band transition.[21] Shown in Fig. 4(d) is the $(ahv)^2 - hv$ plot. The linear relationship between $(ahv)^2$ and hv indicates that CSO has a direct energy bandgap. The optical direct bandgap is estimated to be 3.6 eV by extending the straight portion of the curve. This value is in the reported proximity of 3.3–3.75 eV.[14, 22, 23]

3.4 Hall effect measurement at low temperature

As well as the high infrared transparency, CSO film on a-plane sapphire substrate exhibits good electric conductive characteristic. The temperature dependences of the electrical resistivity, carrier concentration, and Hall mobility of the film were measured between 90 and 300 K, as shown in Fig. 5. The temperature dependence of the electrical transport properties of the film exhibited similar semiconducting characteristics as those of the CSO[3R](0001) epitaxial film.[22,24] The increase in the carrier concentration and the decrease in the Hall mobility and electrical resistivity of the film

were observed with increasing temperature. The Hall coefficient of the CSO film is +5.57 cm^3C^{-1} at room temperature, indicating p-type conduction characteristic.The electrical resistivity, carrier concentration, and Hall mobility of the CSO film at room temperature are 1.047 Ω•cm, 1.12×10^{17} cm^{-3} and 53.2 $cm^2V^{-1}s^{-1}$, respectively, which are highly improved than the previous reports.[14, 24, 25] This suggests that the PAD processing significantly improves the electrical resistivity and Hall mobility of our p-type CSO film.

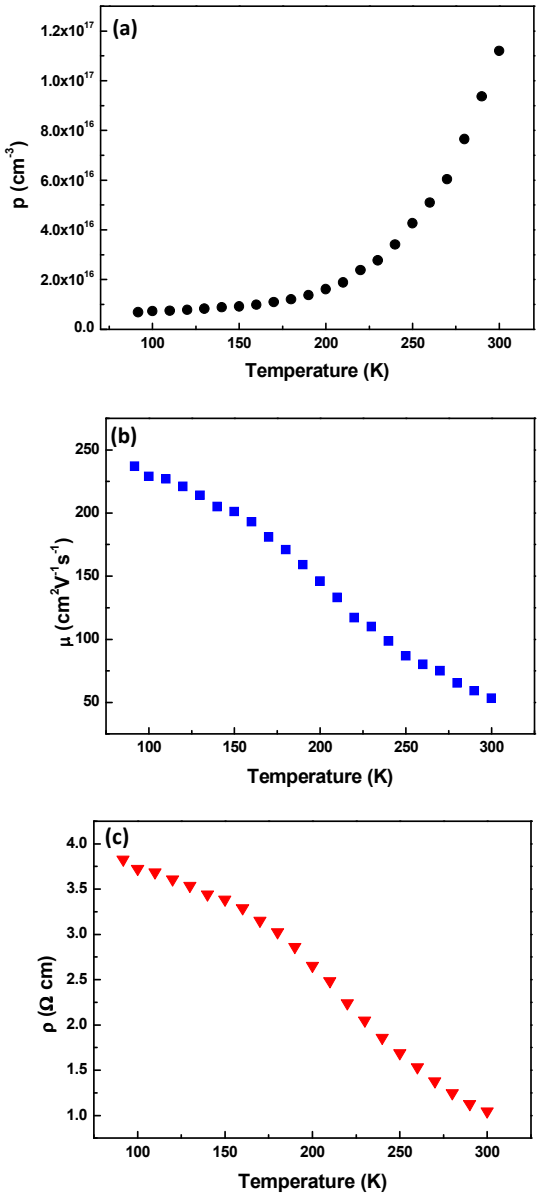

Fig. 6.Temperature dependence of (a) carrier concentration (p), (b) Hall mobility (μ), (c) electrical resistivity(ρ) of CSO thin film.

In order to apply CSO thin film in the application of optoelectronics, it is desired to further enhance its p-type conductivity. Doping CSO with Mg and oxygen intercalation are two effective ways. Mg-doped CSO thin film can be grown by mixing different PAD precursor solutions. A solution containing Cu^{2+}, Sc^{3+} and Mg^{2+} can be prepared as follows: Cu^{2+} is bound to PEI, Sc^{3+} and Mg^{2+} are bound to PEI as an EDTA complex. The metal ions' concentrations of the precursor solutions can be determined by inductively coupled plasma atomic emission spectroscopy. With an accurate control on the metal ions' concentrations, a desired solution can be achieved. The mixture is then coated onto a substrate and thermally annealed. As for the oxygen intercalation, the derived CSO thin film annealed over about one hour under a reasonable oxygen partial pressure, will be feasible to realize the oxygen intercalation of CSO thin film.

3.5 Comparison and discussions

A comparison is made among the proposed PAD method and other two methods, i.e. PLD [14] and TPE [15], in terms of fabrication limitation, optical properties and electrical properties of CSO film, as shown in Table 1. We can draw the following conclusion from the comparison. a) On the aspect of fabrication limitation, all the three methods require high anneal temperature (above 1000 °C), and it will limit the application of CSO in optoelectronic devices which use normal glass or polymer as the substrate; compared with PAD, the other two methods are more suitable for fabricating small-area film, and they both need high-vacuum deposition environment; also, the instrument requirements of PLD and TPE are higher and stricter than that of PAD. In contrast to PLD and TPE, PAD is a simple and cost-effective method, which is capable of synthesizing large-area films, especially for doped film. b) In terms of optical property, the film obtained by PLD possesses higher transmittance in the visible and near-IR bands, and the film obtained by PAD tends to have an outstanding transmittance in the mid-IR band in addition to the visible and near-IR bands. c) From the provided data in Table 1, the electrical resistivity of the film by PAD is six orders lower than that of the film by PLD, suggesting a good conductivity of such film made from PAD technique.

Tab. 1. Comparison among the proposed PAD method and other two methods used for fabricating CSO film [14, 15]

Method	Fabrication limitation	Optical property	Electrical Resistivity (room temperature)
PAD (this)	High anneal temperature (1050 °C);	40-65%, visible; 65-85%, near-IR; >85%, mid-IR band.	1.047 Ω•cm
PLD [14]	Small area; High vacuum; High anneal temperature (1150 °C);	65-90%, visible; 80-90%, near-IR;	9.33×10^6 Ω•cm
TPE [15]	Small area; High vacuum; High anneal temperature (1150°C)	sharp near-band edge photoluminescence at 3.3 eV	not available

4 Conclusions

In summary, in terms of PAD technique, we have, for the first time, grown single phase, large-area, p-type infrared transparent conductive CSO thin film on a-plane sapphire substrate. The unique chemistry and processing design of PAD deliver stable and homogeneous solutions at a molecular level that allows the epitaxial growth of high-quality thin films. The obtained CSO thin film shows promise as transparent electrodes because of

their superior infrared transparency and excellent conductivity. These unique photoelectric properties make the CSO film a promising candidate for use in window electrodes for displays, solar cells, pyro electric detectors, organic light-emitting-diodes (OLEDs) and other novel applications over a wide range of wavelengths.

Acknowledgements

This work was supported in part by the National Natural Science Foundation of China (nos. 11404129, 61307124), National Key Technology R&D Program (nos. 2013BAK06B04, 2014BAD08B03), Science and Technology Department of Jilin Province (no. 20140307014SF), Changchun Municipal Science and Technology Bureau (nos. 11GH01, 14KG022) and the State Key Laboratory of Integrated Optoelectronics, Jilin University (no. IOSKL2012ZZ12).

References

1 A. Kudo, H. Yanagi, K. Ueda, H. Hosono, H. Kawazoe and Y. Yano, Appl. Phys. Lett., 1999, 75, 2851.
2 S. P. Harvey, T. O. Mason, Y. Gassenbauer, R. Schafranek and A. Klein, J. Phys. D: Appl. Phys., 2006, 39, 3959.
3 H. Hosono, Int. J. Appl. Ceram. Technol., 2004, 1, 106.
4 D. S. Hecht, L. B. Hu and G. Irvin, Adv. Mater., 2011, 23, 1482–1513.
5 H. Kawazoe, M. Yasukawa, H. Hyodo, M. Kurita, H. Yanagi and H. Hosono, Nature, 1997, 389, 939.
6 M. S. Lee, T. Y. Kim and D. Kim, Appl. Phys. Lett., 2001, 79, 2028.
7 Y. H. Chuai, B. Hu, Y. D. Li, H. Z. Shen, C. T. Zheng and Y. D. Wang, J. Alloy. Compd., 2015, 627, 299-306.
8 K. Ueda, T. Hase, H. Yanagi, H. Kawazoe, H. Hosono, H. Ohta, M. Orita and M. Hirano, J. Appl. Phys., 2001, 89, 1790.
9 H. Hiraga, T. Makino, T. Fukumura, A. Ohtomo and M. Kawasaki, Appl. Phys. Lett., 2009, 95, 211908.
10 R. Kykyneshi, B. C. Nielsen, J. Tate and A. W. Sleight, J. Appl. Phys., 2004, 96, 6188.
11 J. Li, A. F. T. Yokochi and A. W. Sleight, Solid State Sci., 2004, 6, 831.
12 S. Gilliland, J. F. Sánchez-Royo, J. Pellicer-Porres, A. Segura, A. Muñoz, P. Rodrígues-Hernández and J. López-Solano, Thin Solid Films, 2008, 516, 1431.
13 Q. X. Jia, T. M. McCleskey, A. K. Burrell, Y. Lin, G. E. Collis, H. Wang, A. D. Q. Li and S. R. Foltyn, Nat. Mater., 2004, 3, 529.
14 Y. Kakehi, K. Satoh, T. Yotsuya, S. Nakao, T. Yoshimura, A. Ashida and N. Fujimura, J. Appl. Phys., 2005, 97, 083535.
15 Y. Matsubara, T. Makino, H. Hiraga, C. Chen, S. Tsukimoto, K. Ueno, Y. Kozuka, Y. Ikuhara and M. Kawasaki, Appl. Phys. Express, 2012, 5, 011201.
16 B. J. Ingram, G. B. González, T. O. Mason, D. Y. Shahriari, A. Barnabè, D. Ko and K. R. Poeppelmeier, Chem. Mater., 2004, 16, 5616.
17 G. F. Zou, J. Zhao, H. M. Luo, T. M. McCleskey, A. K. Burrell and Q. X. Jia, Chem. Soc. Rev., 2013, 42, 439.
18 J. Ghijsen, L. H. Tjeng, J. Van Elp, H. Eskes, J. Westerink, G. A. Sawatzky and M. T. Czyzyk, Phys. Rev. B, 1988, 38, 11322.
19 Li-Jie Shi, Zhi-Jie Fang and Jingbo Li, J. Appl. Phys., 2008, 104, 073527.
20 A. D. LaForge, material. Phys. Rev. B, 2010, 81, 125120.
21 Z. Deng, X. Fang, S. Wu, Y. Zhao, W. Dong, J. Shao and S. Wang, J. Alloys Comp., 2013, 577, 658–662.
22 Y. Kakehi, K. Satoh, T. Yotsuya, K. Masuko , T. Yoshimura, A. Ashida and N. Fujimura, J. Cryst. Growth, 2009, 311, 1117–1122.
23 N. Duan, A. W. Sleight, M. K. Jayaraj and J. Tate, Appl. Phys. Lett., 2000, 77, 1325.
24 Y. Kakehi, K. Satoh, T. Yoshimura, A. Ashida and N. Fujimura, Thin Solid Films, 2010, 518, 3097–3100.
25 Y. Kakehi, K. Satoh, T. Yoshimura, A. Ashida and N. Fujimura, Vacuum, 2010, 84, 618–621.